Materials Advances

ROYAL SOCIETY OF CHEMISTRY

PAPER

View Article Online
View Journal | View Issue

Cite this: *Mater. Adv.*, 2025, 6, 5056

Near blue light emitting benzimidazol-2-thione†

Bikash Lahkar, ‡[a] Gopendra Muduli, ‡[a] Suman Mandal,‡[a] Arushi Rawat,[b] Abhilash Sahu, [b] Kohsuke Matsumoto, [b] Osamu Tsutsumi [b] and Ganesan Prabusankar *[a]

Received 10th April 2025,
Accepted 4th June 2025

DOI: 10.1039/d5ma00344j

rsc.li/materials-advances

The discrete organosulfur molecule possessing a high quantum yield with blue luminescence properties has significant potential as an optically active material for future applications. In this context, the sulfoxide or sulfone-based fused heterocyclic materials are known as the new generation of luminogens. The first sulfur-fused heterocyclic thioketone luminogen consisting of a donor–acceptor structure has been reported in this work, with benzimidazole and sulfur acting as the donor, whereas anthracene and pyridine moieties act as the acceptor. Herewith, we report the synthesis of 1-(9-methyl anthracene)-2-(2-methyl pyridine)-benzimidazol-2-thione (**APBT**). The donor and acceptor are connected through a methyl linker. Molecule **APBT** emits at λ_{em} = 494 nm in the crystalline state and λ_{em} = 410 nm in the solution state. Besides, molecule **APBT** showed an aggregation-induced emission due to its molecular packing in the crystalline state. The molecule emits in the near blue region in the crystalline state with a quantum yield of 17.82% and a luminescent lifetime of 47.19 ns. The light-emitting behaviour of crystalline **APBT** is comparable with **APBT**-coated LED. DFT calculations were performed to determine the energy of frontier molecular orbitals, and the HOMO–LUMO gap (HLG) was found to be 3.45 eV.

Introduction

Sulfur is one of the vital elements present in Earth's crust for various biological applications in living organisms.[1] The history of luminescence goes back to the unintentional discovery of Bolognian stone containing BaS, the first sulfide phosphor ever discovered.[2] Thereafter, in 1700, CaS phosphor was developed by Friedrich Hoffmann and followed by SrS phosphor by J. F. John in 1817. Due to its natural abundance and reactivity, it has been utilised in various pharmaceutical and material applications.[3,4] One of the major contributions of sulfur is towards the organic semiconductors for light-emitting device applications.[5–7]

The sulfoxide or sulfone-based fused heterocyclic materials have been extensively investigated as the new generation of luminogens for OLED applications.[8,9] Because of the presence of the two lone pairs and the empty d-orbital in organo sulfur materials, suitable materials can be designed with electron transportation or electron injection properties.[10] Due to such excellent properties, various sulfur-containing chromophores have been studied widely, namely **DBT** (Dibenzothiophene), **DPS** (Diphenyl sulfones), and **BZ**/**NZ** (Thiadiazole) were isolated with sp^3 hybridized sulfur center (Scheme 1). **DBT** with a rigid structure is used as an electron-rich donor, while **DPS** with distorted confirmation is often used as a classical electron acceptor for blue-emitting materials.[11,12] However, **BZ** and **NZ** have been commonly used chromophores for hot excitons.[13] Also, these sulfur-containing materials are well known to possess special phenomena like aggregation-induced emission (AIE), solvatochromism, mechanochromism *etc.*[14] In 2024, Frederic and co-workers have isolated benzo[4,5]thieno-*S*,*S*-dioxide-[3,2-*b*]benzofuran (**BTOBF**) based compounds showcasing an excellent quantum yield of 83% in the solution state and 63% in the crystalline state.[15] However, fused heterocyclic thioketone luminogens with a donor–acceptor structure have not been isolated yet. Because of the large π-conjugation and high quantum yield and the access modification of their structures, fused ring systems are gaining enormous popularity in organic luminescent materials.[16]

Herewith, we report the first sulfur-fused heterocyclic thioketone luminogen, which consists of a donor–acceptor structure. A discrete benzimidazol-2-thione compound 1-(9-methyl anthracene)-2-(2-methyl pyridine)-benzimidazol-2-thione (**APBT**) has been synthesized and characterized. The photophysical

[a] *Organometallics and Materials Chemistry Lab, Department of Chemistry, Indian Institute of Technology Hyderabad, Kandi, Sangareddy, Telangana, 502285, India. E-mail: prabu@chy.iith.ac.in*
[b] *Department of Applied Chemistry, Ritsumeikan University, Kusatsu, 525-8577, Japan. E-mail: tsutsumi@sk.ritsumei.ac.jp*

† Electronic supplementary information (ESI) available: FT-IR, NMR, SCXRD, PXRD, PL, DSC, HRMS, DFT, TD-DFT. CCDC 2435269. For ESI and crystallographic data in CIF or other electronic format see DOI: https://doi.org/10.1039/d5ma00344j

‡ These authors contributed equally.

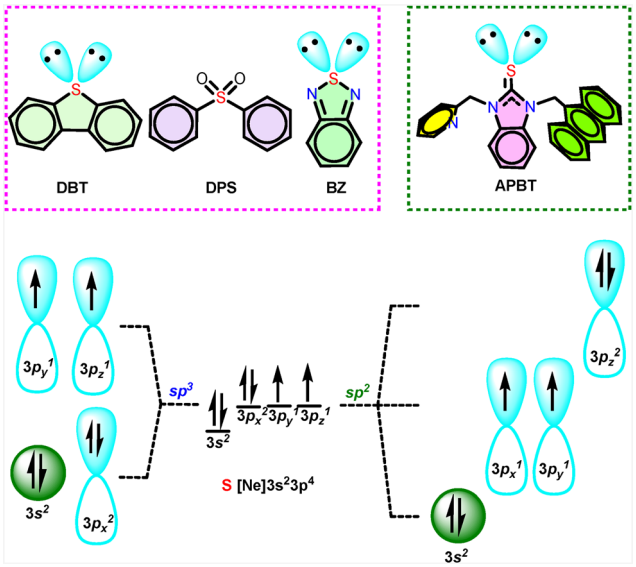

Scheme 1 Schematic representation of orbital splitting in different hybridizations of S atom.

properties of the molecule were examined, and an LED demo was also shown. Besides, the theoretical calculations were carried out to understand the structural and electronic properties.

Results and discussion

APBT was synthesized using the standard Schlenk technique under an argon atmosphere to ensure an inert environment during the chemical reactions. **APBT** was prepared by reacting 1-(9-methyl anthracene)-2-(2-methyl pyridine)-benzimidazolium chloride salt, K_2CO_3 as a base, and sulfur in the presence of methanol as a solvent under reflux conditions (Scheme 2). It was characterized by HRMS, ^{1}H NMR, ^{13}C NMR, FT-IR, PXRD, and SCXRD. From the ^{1}H NMR, the disappearance of the imidazo N–C*H*–N proton is observed. In the ^{13}C NMR, the characteristic *C*═S peak is observed at 170.2 ppm. This confirms the formation of the product by the NMR technique.[17] The specific stretching frequency of C═S, which appeared at 1220 cm^{-1} was observed in the FT-IR spectrum (see ESI,† Fig. S1–S4).

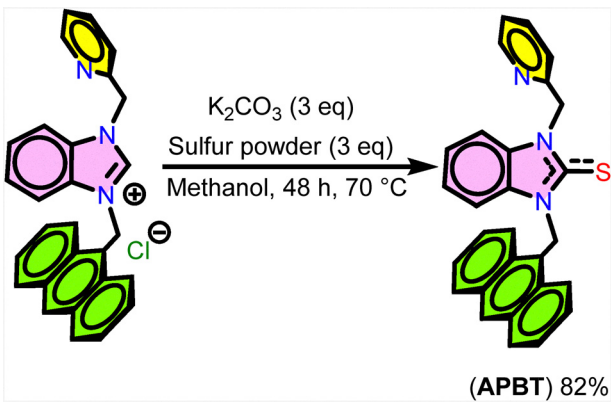

Scheme 2 Synthesis of **APBT**.

A single crystal of **APBT** was isolated from a saturated DCM solution. Single crystal X-ray diffraction technique (SCXRD) was used to determine the crystalline-state structure of **APBT** (Fig. 1). It was crystallized in the triclinic crystal system with the space group $P\bar{1}$. The C1–S1 bond length in the molecule is 1.671(14) Å, which is comparable to the bond lengths of thione molecules reported in the literature.[17] The structural parameters of **APBT** have been summarised in the ESI† (see ESI,† Table S1). The bond angle between N1–C1–S1 is 126.26(10)°. The bulk phase sample purity was determined by comparing the simulated powder pattern with the experimental powder XRD pattern (see ESI,† Fig. S5).

The packing diagram of **APBT** showed intermolecular CH···π interactions ranging from 2.586 Å to 4.401 Å between the methylene proton linked with pyridine and anthracene π ring (Fig. 2).[18] Also, an intermolecular interaction (2.931 Å) exists between sulfur and hydrogen.[19,20] This type of interaction is called sulfur-centered hydrogen bonding interaction (SCHB) and is comparable to the similar interactions reported.[21,22] The percentage buried volume (%V_{bur}) and topographic steric map of **APBT** were calculated (see ESI,† Fig. S6).[23]

The solid-state structure of the molecule suggests the presence of several interactions such as S···H, CH···CH, CH···π. It was designed by incorporating anthracene, pyridine, and sulfur groups into benzimidazole. An investigation was carried out to achieve greater insight into geometries, electronic properties, and electronic transitions for **APBT**. A comprehensive DFT computational study was carried out with the help of the B3LYP/6-31G(d,p) basis set. The ground state optimized geometry of **APBT** is comparable to that of the experimental X-ray crystallography structure as shown in Fig. 1. The interactions between sulfur and hydrogens

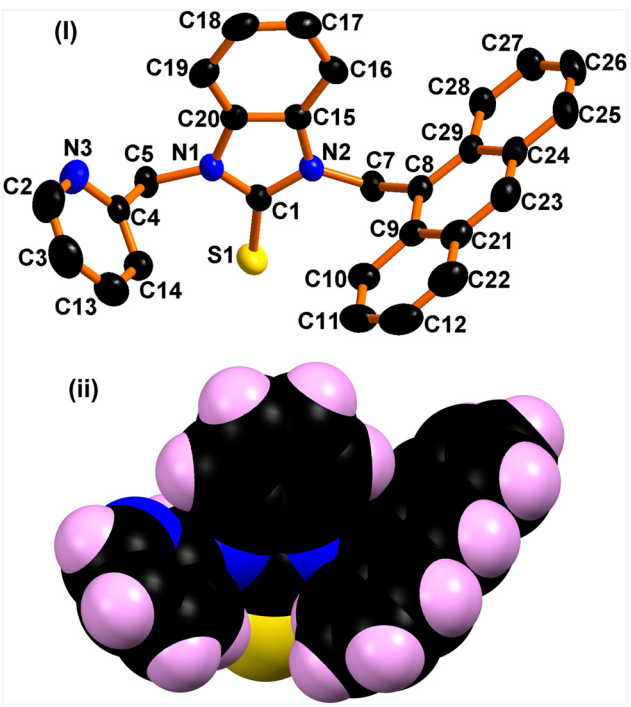

Fig. 1 (i) Solid state structure of **APBT**. (ii) Space-filling model of **APBT**.

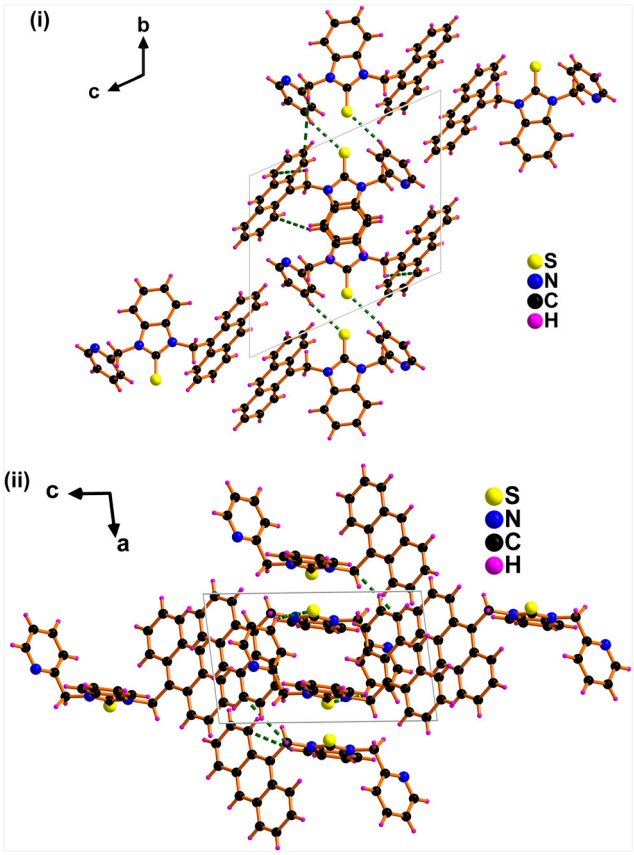

Fig. 2 Solid-state packing of **APBT** consists of (C)S···H and CH···π interactions (i) view along *a* axis. (ii) View along *b* axis.

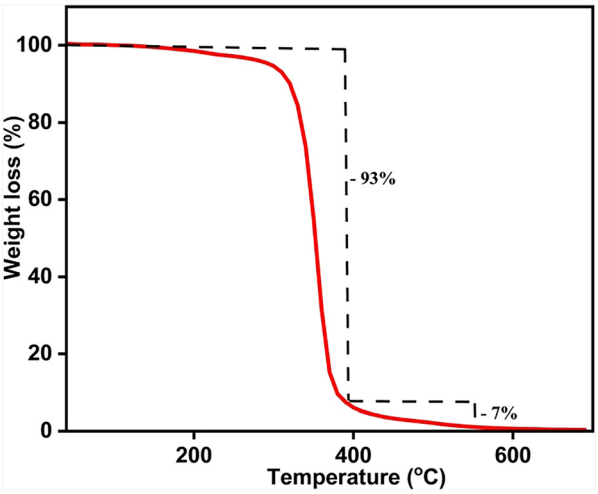

Fig. 3 TGA plot of **APBT** at a heating rate of 10 °C minute^{-1}.

get contracted to stabilize the molecule. The excited state energy of the molecule was calculated using the TD-SCF method by taking a well-optimized geometry of **APBT**. The ground state electronic clouds of the molecule can be seen from the ESP map with the most negative potential (red color), positive potential (blue color), and neutral potential (green and yellow) (see ESI,† Fig. S7). To discuss more intramolecular interactions in the crystal of **APBT**, topology analysis, and RDG-NCI analysis were carried out and the results are shown. (See ESI,† Fig. S8 and S9). The intramolecular S···H interactions show several bond critical points. They are mostly noncovalent characters. The Lagrangian kinetic energy at the bond critical points $G(r)$ between sulfur and hydrogen is greater than the potential energy density $V(r)$. The ratio of $|G(r)|/V(r)|$ is greater than or equal to 1, confirming the noncovalent nature and interactions mainly showing the van der Waals in nature.

The crystal structure of **APBT** and the packing diagram suggested checking the Hirshfeld surface analysis. The surface and its fingerprint plots were used to measure the intramolecular as well as intermolecular interactions. The Hirshfeld surface computation was carried out using Crystal Explorer 21.5 software.[24] The term d_e and d_i refers to the closest distance from the Hirshfeld surface to molecules on the outside and inside (see ESI,† Fig. S18). The major intermolecular interaction (~50.7%) occurs through hydrogen bonds H···H at a distance of $d_e \sim 2.033$ Å. The second main interaction (~28.4%) can be seen for C···H/H···C with a distance range of 2.695 Å. The S···H/H···S interaction accounts for ~8.2% of the Hirshfeld area in the range of 2.816 Å. Also, various other weak interactions have been identified by mapping shape index, curvedness, fragment patch, *etc.*

The thermal stability of **APBT** was investigated by the thermogravimetric analysis (TGA) technique at a heating rate of 10 °C per minute at a temperature ranging from 30 to 700 °C (Fig. 3). The molecule shows decomposition in a single-step process. The molecule starts to decompose after 210 °C, leaving only the sulfur in the system until 400 °C (93% weight loss). This sulfur was also removed from the system at a temperature above 400 °C, which is around 7% (cal: 7.3%).[25] The melting point of **APBT**, which is 220 °C, was obtained using the differential scanning calorimetry (DSC) technique (see ESI,† Fig. S10).

The photophysical characteristics of the molecule were studied. The UV-vis measurement was conducted in 1×10^{-5} M DCM solution (Fig. 4). The λ_{abs} of **APBT** were at 257 nm in DCM, which is due to the n → π* transition from the nitrogen center of the imidazole ring to the anthracene moieties (Table 1). The λ_{abs} peak appearing at 312 nm can be accredited for π → π* transition arising from the π conjugation of the aromatic rings. The shoulder peaks at 368 nm to 390 nm arise due to intra-ligand charge transfer.[26]

The emission spectrum of the molecule solution state was obtained in (1×10^{-5} M) DCM solution and compared with the crystalline-state emission spectra that were measured using single crystals of the molecule. In the solution state, the λ_{em} = 410 nm (excitation at 262 nm), which gets red-shifted to λ_{em} = 494 nm in the crystalline state (excitation at 285 nm) (Fig. 4 and Table 1). This is due to the difference in packing in the crystalline state. The emission arises due to the extended conjugation of the polyaromatic anthracene ring and also because of the intra-ligand charge transfer facilitated by the sulfur atom.

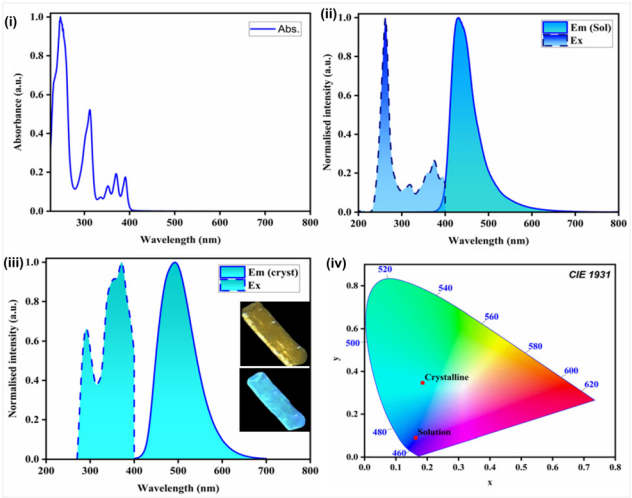

Fig. 4 (i) UV-Vis spectrum of **APBT** in DCM at RT ($C = 1 \times 10^{-5}$ M); (ii) emission spectrum of **APBT** (λ_{ex} = 262 nm) in DCM at RT ($C = 1 \times 10^{-5}$ M); (iii) emission spectrum of **APBT** (λ_{ex} = 285 nm) as single crystals at RT; (iv) CIE diagram of **APBT** in crystalline and solution state.

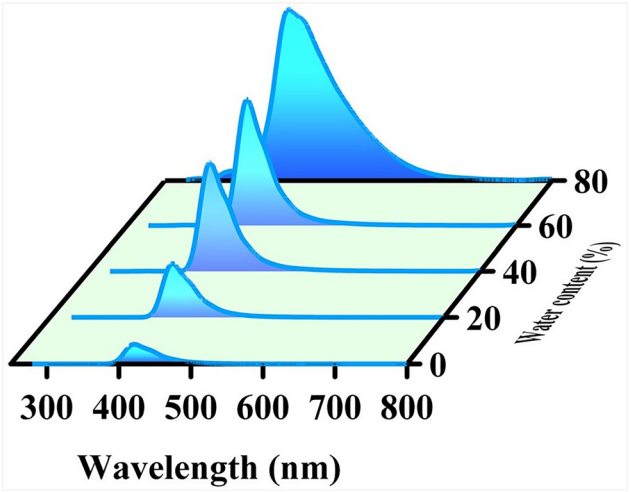

Fig. 5 Emission of **APBT** in THF in different water percentages. Increases water content from front to back.

The photoluminescence quantum yield (PLQY) of **APBT** in DCM solution was calculated relative to the standard fluorophore anthracene in ethanol. The fluorescence quantum yield is 5.41%. The lifetime decay profile was found in the nanosecond range of τ_{avg} of 2.14 ns in DCM solution. Similarly, PLQY in the crystalline state was acquired using single crystals of **APBT** at RT. We observed a good quantum yield of 17.82%. The lifetime data was collected using the time-correlated single photon counting technique (TCSPC). The nanosecond decay profile was observed for the molecule (τ_{avg} = 47.19 ns). The obtained quantum yield of the **APBT** molecule in the crystalline state is found to be better than the previously reported thiophene-bridged macrocyclic pseudo-meta[2.2]paracyclophanes.[27] The decay profile of **APBT** is fitted by a biexponential decay curve, and the nanosecond decay curve corresponds to fluorescence. The radiative rate constant (k_r) was found to be 3.7×10^6 s^{-1} for fluorescence. This corresponds to the emission corresponding to the transition from the $S_1 \rightarrow S_0$ state. The quantitative evaluation of the photoluminescence color was estimated with the Commission Internationale de L'Eclairage (CIE) plot. The CIE coordinates of observed emission in the solution state are x = 0.1594, y = 0.0468 while the emission color in the crystalline state is near blue with coordinates x = 0.1855, y = 0.3464.

To study the solvatochromism and mechanochromism behavior of **APBT**, we have taken solution state emission in various organic solvents ($C = 1 \times 10^{-5}$ M), and it is found that there is no considerable change in the emission behavior of the molecule in varying the solvent (see ESI,† Fig. S11). There is also no such change in the emissive property of the molecule under mechanical stress when we compared the emission of the crystalline sample and the ground powder sample (see ESI,† Fig. S12).

An investigation of the AIE (aggregation-induced emission) behavior of **APBT** in different water ratios in the THF solution was performed (Fig. 5). This investigation reveals a 10 nm red shift in the emission of **APBT** in 80% water in the THF solution as compared to a lower water percentage (λ_{ex} = 262 nm).[28,29] Notably, the emission intensity of **APBT** increases when we increase the content of water, decreasing the volume of **APBT** in THF. The emission spectra of **APBT** in 80% water content broadened towards the red region.

The above-mentioned AIE phenomena can be enlightened by the RIM mechanism (restriction of intramolecular motion).[30] In the solution state, the molecules of **APBT** experienced minimal intermolecular interaction with each other when encircled by the solvent molecules. Therefore, upon excitation in the solution state, they de-excited back to the ground state *via* non-radiative (NR) processes, causing lesser emission. But in the presence of excess water, the hydrophobic molecules of **APBT** start to aggregate. This induces a steric effect which restricts the free motion of the molecules, prevents the non-radiative processes, and produces comparatively higher emissions.

The frontier molecular orbital energy was explored to gain an idea about the HOMO and LUMO (Fig. 6 and Table 2). The corresponding key parameters are shown in Table S3 (ESI†) from DFT calculations. The singlet–triplet energy levels were also calculated from TD-DFT. Energy for S_1 and T_1 are found to be 2.947 eV and 1.745 eV, respectively, and their difference

Table 1 Photophysical parameters of APBT at room temperature in DCM solution ($C = 1 \times 10^{-5}$ M) and crystalline state

λ_{abs} [a] (nm)	λ_{ex} [a] (nm) (Sol.)	λ_{em} [a] (nm) (Sol.)	λ_{ex} [b] (nm) (Crys.)	λ_{em} [b] (nm) (Crys.)	τ_{avg} [b] (ns)	Φ_{PL} [b] (%) (Crys.)	k_r [b] (s^{-1})	k_{nr} [b] (s^{-1})
257, 312, 368, 390	262	410	285	494	47.19	17.82	3.70×10^6	18.06×10^6

[a] DCM ($C = 1 \times 10^{-5}$ M) solution. [b] Crystalline state.

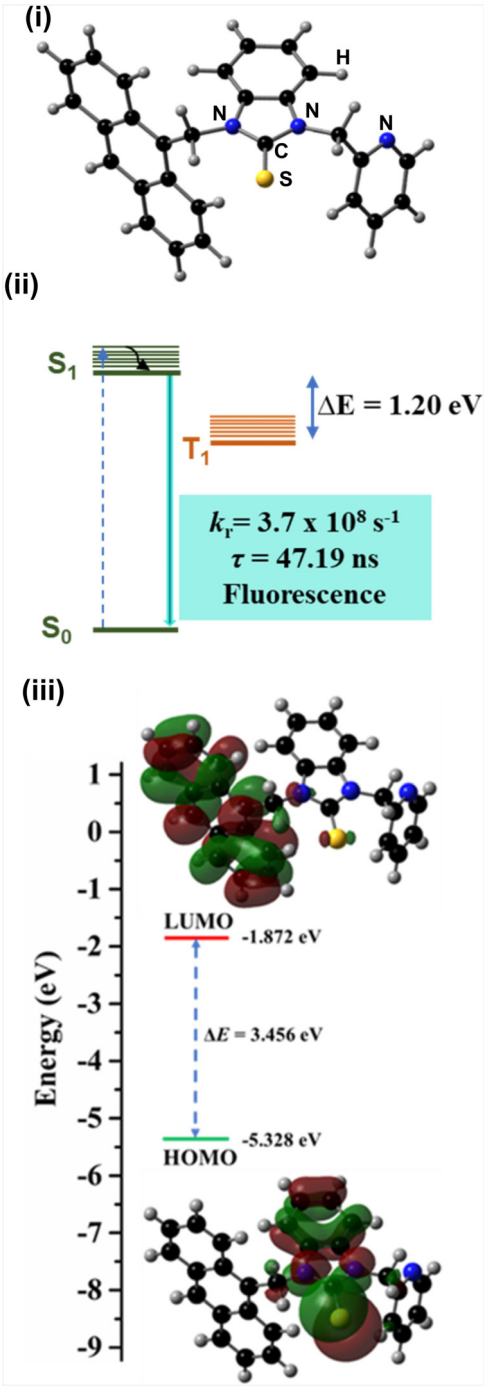

Fig. 6 (i) Optimized geometry of **APBT**. (ii) The proposed decay scheme of LLCT. (iii) HOMO–LUMO energy gap of **APBT**.

(ΔE_{ST}) is 1.202 eV. The main distribution at the HOMO is appearing from the electron-donating benzimidazole–thione moiety. The LUMO is found in the electron-accepting anthracene unit. The energy level of HOMO and LUMO are −5.32 eV and −1.87 eV, respectively. The HOMO–LUMO gap (HLG) is found to be 3.45 eV. The vertical transitions were determined by using time-dependent DFT (TD-DFT). The simulated UV-vis spectra were calculated to compare with the experimental value (see ESI,† Fig. S13).

Table 2 The calculated total energy and HOMO–LUMO gap

Total energy	−1642.15196293 a.u.
Dipole moment	3.6444 Debye
E_{HOMO} (eV)	−5.328
E_{HOMO-1} (eV)	−5.359
E_{LUMO} (eV)	−1.872
E_{LUMO+1} (eV)	−0.844
HLG (eV)	3.456
Total energy	−1642.15196293 a.u.

The electrochemical characteristics of **APBT** were examined using cyclic voltammetry in a 5 mM DMF solution. An Ag/AgCl electrode served as the reference, with platinum as the working electrode and carbon as the counter electrode. The compound showed a reversible one-electron oxidation, with a half-wave potential ($E_{1/2}$) of 0.20 V. The oxidation and reduction peak potentials were observed at 0.51 V and −0.09 V, respectively, resulting in an electrochemical energy gap of 0.61 V (see ESI,† Fig. S21). The HOMO and LUMO energy levels were found to be −4.91 eV and −4.30 eV. This significant deviation from the DFT calculated HOMO–LUMO gap can be due to the absence of non-covalent or secondary interactions in the solution state.

To further demonstrate the application of such light-emitting molecules in the synthesis of LEDs, we have coated the compound on the surface of a commercially available 3 V LED bulb (λ_{em} = 410 nm) by using a THF solution of polymethyl methacrylate (PMMA) and **APBT** in 1 : 10 ratio by weight (Fig. 7). The advantages of using PMMA as a binding agent arise from its cost-effectiveness and its low optical absorbance capacity. The emission spectrum of the coated LED is obtained, and it shows emission from λ_{em} = 428 to 600 nm in the bluish-green region with emission maxima at λ_{em} = 470 nm. The coated LED emission spectrum shows a very weak peak at λ_{em} = 410 nm, showing the presence of minimal emission from the LED where the molecule **APBT** was coated. The emmision of coated LED is nearly comparable to that of crystalline **APBT**. This near-blue emitting molecule can be used for the synthesis of white LEDs by mixing with red and green emitting molecules.

Experimental

Methods and materials

All reactions have been performed using a standard Schlenk technique under an inert atmosphere to ensure an inert environment during the chemical reactions. The starting materials 9-anthracenemethanol, benzimidazole, and 2-picolyl chloride were obtained from commercial sources. Before use, the solvent underwent a drying and distillation process per industry standards. The NMR spectra were recorded on a Bruker Ultra Shield 400 MHz spectrometer at 25 °C. FT-IR data were obtained utilizing the ATR technique with a Bruker Alpha-P Fourier Transform Spectrometer. Suitable single crystals of **APBT** were acquired from a solution of DCM. Bruker D8 Venture Single Crystal X-ray diffractometer was used to obtain the crystal structure of **APBT** using the source Mo-K_α (0.71073 Å) at 298 K. Olex2.solve was used to solve the structures, and the

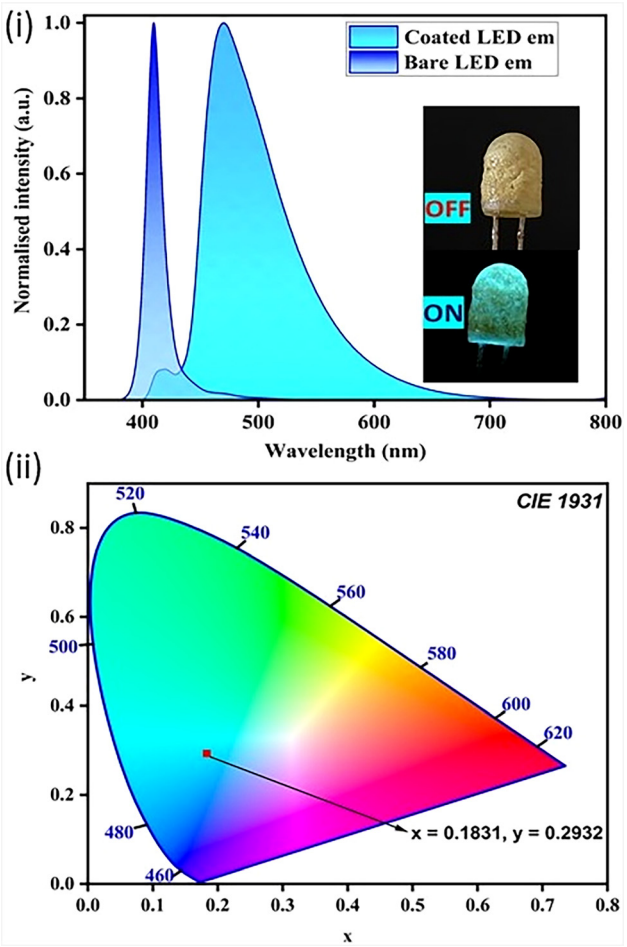

Fig. 7 (i) The prototype LED demo with emission spectrum (λ_{ex} = 410 nm); (ii) CIE diagram of its emission.

Charge Flipping method was used to solve them.[31] The structures have been refined using the Gauss–Newton minimization method with the Olex2 refinement package.[32] Powder X-ray diffraction was attained utilizing a Rigaku Ultima IV instrument. The thermal stability study was carried out using the TA-SDT-Q600 instrument. UV-Vis Spectrometer LAB INDIA 2000 U was used to record electronic spectra, while the Hitachi F-4700 fluorescence spectrophotometer was used to acquire emission spectra. Quantum yield of **APBT** in DCM was determined relative to standard anthracene in ethanol with a QY of 27%. The refractive index of solvents was taken care of. All samples were diluted to ensure absorbance less than 0.1. The photoluminescence quantum yield (Φ) in the crystalline state was measured using a Hitachi F-7000 fluorescence spectrophotometer using a calibrated integration sphere system (Hitachi, Tokyo, Japan) using alumina oxide as the standard reference. Photoluminescence decay profiles were measured by using Quantaurus-Tau (Hamamatsu) and Hitachi Fluoromax4. The AUTOLAB 302 Modular Potentiostat electrochemical analyser was used to perform cyclic voltammetry (CV) of **APBT** at 298 ± 1 K. Three standard electrode configurations—a glassy carbon working electrode, a platinum plate auxiliary electrode, and an Ag/AgCl reference electrode—were used to maintain the scan rate at 20 mV s^{-1} during the tests, which were conducted in dimethylformamide (DMF) with 0.1 M tetrabutylammonium perchlorate (Bu_4NClO_4) as a supporting electrolyte.

Computational methodology

The CIF file of **APBT** from X-ray crystallography has been utilized for computational studies. The density functional theory (DFT) for the ground state and time-dependent density functional theory (TD-DFT) for the excited states were carried out at the B3LYP function with 6-31G(d,p) basis set for C, H, N, and S using Gaussian16 package. The topological investigation of electron density, reduced density gradient (RDG), and non-covalent interactions (NCI) were analyzed by the Multiwfn program (version 3.8) and the VMD program was utilized for visualization.[33–38]

Preparation of 1-(9-methyl-anthracene)-2-(2-methyl pyridine)-benzimidazol-2-thione (APBT). A mixture of 1-(9-methyl anthracene)-2-(2-methyl pyridine)-benzimidazolium chloride salt (1.00 g, 2.29 mmol), Sulfur (0.22 g, 6.87 mmol) and potassium carbonate (0.95 g, 6.87 mmol) in methanol (15 mL) were refluxed for 48 h at 70 °C. After completion of the reaction, the compound was extracted with DCM. The organic phase was dried over Na_2SO_4, and the desired product was collected under reduced pressure. M.p.: 220–225 °C. Yield: 82% (based on 1-(9-methyl anthracene)-2-(2-methyl pyridine)-benzimidazolium chloride). HRMS *m*/*z*: $[(C_{28}H_{21}N_3S) + H]^+$, calculated for $C_{28}H_{21}N_3S$ 431.17, found 432.15. ^{1}H NMR (400.130 MHz, *J* = Hz, $CDCl_3$) δ_H = 8.47 (1 H, d, *J* = 4.4 Hz, Pyr-*H*), 8.40 (3 H, d, *J* = 8.9 Hz, An-*H*), 7.93 (2 H, d, *J* = 8.3 Hz, An-*H*), 7.54–7.43 (3 H, m, An-*H*, Pyr-*H*), 7.41–7.34 (2 H, m, An-*H*, Pyr-*H*), 7.15 (1 H, d, *J* = 7.8 Hz, Pyr-*H*), 7.07 (1 H, dd, *J* = 7.1, 5.2 Hz, Pyr-*H*), 6.95 (1 H, d, *J* = 8.0 Hz, Ben-*H*), 6.73 (1 H, t, *J* = 7.7 Hz, Ben-*H*), 6.50 (2 H, s, CH_2), 6.41 (1 H, t, *J* = 7.8 Hz, Ben-*H*), 6.00 (1 H, d, *J* = 8.2 Hz, Ben-*H*), 5.71 (2 H, s, CH_2). ^{13}C NMR (101.612 MHz, $CDCl_3$) δ_C = 170.4, (*C*═S), for aromatic carbons 155.8, 149.5, 137.1, 131.5, 131.3, 129.9, 127.2, 125.4, 125.2, 123.0, 122.9, 122.0, 110.7, 109.8, 50.7 (*C*H_2), 44.1 (*C*H_2). FT-IR (cm^{-1}, neat): 3044 (w), 2924 (m), 2154 (w), 2015 (m), 1585 (m), 1480 (m), 1398 (s), 1320 (s), 1220 (m), 1169 (m), 1020 (m), 980 (m), 832 (m), 733 (vs).

Conclusions

We have successfully synthesized and characterized near-blue light-emitting thione molecule **APBT**. The photophysical studies of the molecule were studied. In the solution state, it emits at 410 nm, and in the crystalline state, it emits at 494 nm. The quantum yield of **APBT** was found to be 17.82% with a nanosecond decay profile (τ_{avg} = 47.19 ns), indicating fluorescence type of emission. Subsequently, the LED demo was carried out where the coated LED was emitting at 470 nm. Besides, the DFT calculations were performed, and the HOMO–LUMO gap (HLG) was found to be 3.45 eV, considering the transition from sulfur and benzimidazole groups to anthracene moiety.

Author contributions

BL: conceptualization of the original idea, designing methodology experimental, analysis of data, and writing the manuscript; GM: conceptualization of the original idea, designing methodology experimental, analysis of data, and writing the manuscript; SM: conceptualization of the original idea, designing methodology experimental, analysis of data, and writing the manuscript; AR: conceptualization of the analysis of data, and writing the manuscript; AS: conceptualization of the analysis of data, and writing the manuscript; MK: conceptualization of the analysis of data, and writing the manuscript; OT: conceptualization of the analysis of data, and writing the manuscript; GP: conceptualization of the original idea, supervision, fund acquisition, discussion, review and writing the manuscript.

Conflicts of interest

The authors filed a patent for this work. Application No: 202441074170.

Data availability

Data for this article include FT-IR, NMR, PXRD, crystal images, PL studies, HRMS, and DSC along with crystal data, structure refinement of the reported molecule, and DFT-the data for the ESI.† CCDC 2435269 (**APBT**) contains the supplementary crystallographic data for this paper.

Acknowledgements

GP and BL gratefully acknowledges SERB-CRG CRG/2022/000714, New Delhi, India, for the financial support. SM sincerely thanks MoE, and GM thanks PMRF funding New Delhi, India, for the monetary support.

Notes and references

1 J. Yuan, Z. Xu and M. O. Wolf, *Chem. Sci.*, 2022, **13**, 5447–5464.
2 E. N. Harvey, American Philosophical Society, Philadelphia, 1957.
3 E. A. Ilardi, E. Vitaku and J. T. Njardarson, *J. Med. Chem.*, 2014, **57**, 2832–2842.
4 H. Mutlu, E. B. Ceper, X. Li, J. Yang, W. Dong, M. M. Ozmen and P. Theato, *Macromol. Rapid Commun.*, 2019, **40**, 1800650.
5 S. C. Rasmussen, S. J. Evenson and C. B. McCausland, *Chem. Commun.*, 2015, **51**, 4528–4543.
6 Y. Li, J.-Y. Liu, Y.-D. Zhao and Y.-C. Cao, *Mater. Today*, 2017, **20**, 258–266.
7 K. Takimiya, S. Shinamura, I. Osaka and E. Miyazaki, *Adv. Mater.*, 2011, **23**, 4347–4370.
8 P. F. Smet, I. Moreels, Z. Hens and D. Poelman, *Materials*, 2010, **3**, 2834–2883.
9 Y. Li, W. Li, J. Hu, X. Yao, L. Hua, W. Cai, S. Shi, C. Zhang, Z. Liu, S. Li, X. Chen, Z. Sun, Z. Ren, M. C. Tang, G. Wei and Z. Fei, *Adv. Opt. Mater.*, 2023, **11**, 2300298.
10 Z. Feng, Z. Cheng, H. Jin and P. Lu, *J. Mater. Chem. C*, 2022, **10**, 4497–4520.
11 R. Huang, N. A. Kukhta, J. S. Ward, A. Danos, A. S. Batsanov, M. R. Bryce and F. B. Dias, *J. Mater. Chem. C*, 2019, **7**, 13224–13234.
12 Q. Zhang, J. Li, K. Shizu, S. Huang, S. Hirata, H. Miyazaki and C. Adachi, *J. Am. Chem. Soc.*, 2012, **134**, 14706–14709.
13 J. Liu, Z. Li, T. Hu, X. Wei, R. Wang, X. Hu, Y. Liu, Y. Yi, Y. Y. Takamura, Y. Wang and P. Wang, *Adv. Opt. Mater.*, 2019, **7**, 1801190.
14 J. Guo, X.-L. Li, H. Nie, W. Luo, R. Hu, A. Qin, Z. Zhao, S. J. Su and B. Z. Tang, *Chem. Mater.*, 2017, **29**, 3623–3631.
15 K. Youssef, A. Gasonoo, M. Allain, H. Melville, L. Sanguinet, G. C. Welch and F. Gohier, *ACS Appl. Opt. Mater.*, 2024, **2**, 1610–1618.
16 W. Ma, G. Liu, L. Zhou, B. Li and Y. Wang, *J. Mater. Chem. C*, 2020, **8**, 8796–8803.
17 M. Mannarsamy and G. Prabusankar, *New J. Chem.*, 2021, **45**, 5933–5938.
18 A. Fujii, S. Morita, M. Miyazaki, T. Ebata and N. Mikami, *J. Phys. Chem. A*, 2004, **108**, 2652–2658.
19 A. D. Sherry and K. F. Purcell, *J. Am. Chem. Soc.*, 1972, **94**, 1848–1853.
20 F. Wennmohs, V. Staemmler and M. Schindler, *J. Chem. Phys.*, 2003, **119**, 3208–3218.
21 P. Bhadoria and V. Ramanathan, *J. Phys. Chem. A*, 2023, **127**, 8095–8109.
22 S. Sarkar, M. Monu and B. Bandyopadhyay, *J. Phys. Chem.*, 2019, **21**, 25439–25448.
23 L. Falivene, Z. Cao, A. Petta, L. Serra, A. Poater, R. Oliva, V. Scarano and L. Cavallo, *Nat. Chem.*, 2019, **11**, 872–879.
24 P. R. Spackman, M. J. Turner, J. J. McKinnon, S. K. Wolff, D. J. Grimwood, D. Jayatilaka and M. A. Spackman, *J. Appl. Crystallogr.*, 2021, **54**, 1006–1011.
25 W. F. Faragher, J. C. Morrell and S. Comay, *Ind. Eng. Chem. Res.*, 1928, **20**, 527–532.
26 T. M. Swager, C. J. Gil and M. S. Wrighton, *J. Phys. Chem.*, 1995, **99**, 4886–4893.
27 C. Kress, E. Sidler, P. Downey, P. Zwick, O. Fuhr, D. Fenske, S. Bernhard and M. Mayor, *Chem. – Eur. J.*, 2024, **30**, e202303798.
28 Y. Hong, J. W. Y. Lam and B. Z. Tang, *Chem. Soc. Rev.*, 2011, **40**, 5361–5388.
29 Y. Hong, J. W. Y. Lam and B. Z. Tang, *Chem. Commun.*, 2009, 4332–4353.
30 J. Mei, N. L. C. Leung, R. T. K. Kwok, J. W. Y. Lam and B. Z. Tang, *Chem. Rev.*, 2015, **115**, 11718–11940.
31 O. V. Dolomanov, L. J. Bourhis, R. J. Gildea, J. A. K. Howard and H. Puschmann, *J. Appl. Crystallogr.*, 2009, **42**, 339–341.
32 L. J. Bourhis, O. V. Dolomanov, R. J. Gildea, J. A. K. Howard and H. Puschmann, *Acta Crystallogr., Sect. A: Found. Adv.*, 2015, **71**, 59–75.

33 J. Contreras-García, E. R. Johnson, S. Keinan, R. Chaudret, J.-P. Piquemal, D. N. Beratan and W. Yang, *J. Chem. Theory Comput.*, 2011, **7**, 625–632.
34 E. R. Johnson, S. Keinan, P. Mori-Sánchez, J. Contreras-García, A. J. Cohen and W. Yang, *J. Am. Chem. Soc.*, 2010, **132**, 6498–6506.
35 T. Lu and F. Chen, *J. Comput. Chem.*, 2012, **33**, 580–592.
36 W. Humphrey, A. Dalke and K. Schulten, *J. Mol. Graphics*, 1996, **14**, 33–38.
37 M. J. Frisch, G. W. Trucks, H. B. Schlegel, G. E. Scuseria, M. A. Robb, J. R. Cheeseman, G. Scalmani, V. Barone, G. A. Petersson, H. Nakatsuji, X. Li, M. Caricato, A. V. Marenich, J. Bloino, B. G. Janesko, R. Gomperts, B. Mennucci, H. P. Hratchian, J. V. Ortiz, A. F. Izmaylov, J. L. Sonnenberg, D. Williams-Young, F. Ding, F. Lipparini, F. Egidi, J. Goings, B. Peng, A. Petrone, T. Henderson, D. Ranasinghe, V. G. Zakrzewski, J. Gao, N. Rega, G. Zheng, W. Liang, M. Hada, M. Ehara, K. Toyota, R. Fukuda, J. Hasegawa, M. Ishida, T. Nakajima, Y. Honda, O. Kitao, H. Nakai, T. Vreven, K. Throssell, J. A. Montgomery, Jr., J. E. Peralta, F. Ogliaro and M. J. Bearpark, *Gaussian 16, Revision A.03*, Gaussian, Inc., Wallingford CT, 2016.
38 R. Dennington, T. A. Keith and J. M. Millam, *GaussView, Version 6*, Semichem Inc., Shawnee Mission, KS, 2016.